Nanoscale Advances

ROYAL SOCIETY OF CHEMISTRY

PAPER

View Article Online
View Journal | View Issue

Cite this: *Nanoscale Adv.*, 2023, **5**, 2621

Pd@L-asparagine–EDTA–chitosan: a highly effective and reusable bio-based and biodegradable catalyst for the Heck cross-coupling reaction under mild conditions†

Mohammad Dohendou, Mohammad G. Dekamin * and Danial Namaki

In this research, a novel supramolecular Pd(II) catalyst supported on chitosan grafted by L-asparagine and an EDTA linker, named Pd@ASP–EDTA–CS, was prepared for the first time. The structure of the obtained multifunctional Pd@ASP–EDTA–CS nanocomposite was appropriately characterized by various spectroscopic, microscopic, and analytical techniques, including FTIR, EDX, XRD, FESEM, TGA, DRS, and BET. The Pd@ASP–EDTA–CS nanomaterial was successfully employed, as a heterogeneous catalytic system, in the Heck cross-coupling reaction (HCR) to afford various valuable biologically-active cinnamic acid derivatives in good to excellent yields. Different aryl halides containing I, Br and even Cl were used in HCR with various acrylates for the synthesis of corresponding cinnamic acid ester derivatives. The catalyst shows a variety of advantages including high catalytic activity, excellent thermal stability, easy recovery by simple filtration, more than five cycles of reusability with no significant decrease in its efficacy, biodegradability, and excellent results in the HCR using low-loaded Pd on the support. In addition, no leaching of Pd into the reaction medium and the final products was observed.

Received 25th January 2023
Accepted 17th March 2023

DOI: 10.1039/d3na00058c

rsc.li/nanoscale-advances

1. Introduction

Among different organic transformations, Heck cross-coupling reaction (HCR), also known as Mizoroki–Heck reaction,[1–5] has received significant interest in recent years due to its ability to form C–C bonds. Indeed, this reaction has emerged as an efficient replacement, working under extensively mild conditions, for the Grignard reagents and subsequent required organic transformations to construct C=C bonds. Green chemistry (GC) has significant effects on the improvement of human civilization.[6–9] For this reason, developing chemical reactions according to the GC metrics in terms of the use of well-dispersed heterogeneous, bio-based, and biodegradable catalytic systems is vital.[10–13] Therefore, they have had a impressive and critical role in chemical synthesis to make a revolution in synthetic organic chemistry. Due to the different applications of HCR in the organic synthesis and manufacturing of important products such as agrochemicals[14] and active pharmaceutical ingredients (APIs),[15] the progress to develop effective approaches for HCR especially in the pharmaceutical industry is fundamental.[16–20] Definitely, catalytic systems have played a key role in this reaction; consequently, the preparation of useful and applicable catalysts in this field is very important. Recently, various heterogeneous Pd catalysts have been used in the HCR and other cross-coupling reactions, which have shown more advantages compared to homogeneous counterparts such as precluding the addition of different ligands, no Pd leaching in the final products, easy recycling and separation of over-priced Pd from the reaction medium, and reasonable application in industrial sectors.[21–37] Subsequently, from the greenness, cost-effectiveness, and safety point of view, it is essential to develop simple and effective procedures for the HCR by means of heterogeneous Pd catalysts.[31,38–46]

Heterogeneous metal catalysts are normally produced through the chelation of metal nanoparticles (NPs) on suitable solid supports and can simplify the separation and recovery of both catalysts and desired products from the reaction medium.[34,47–50] As a result, to design and produce an effective catalyst, the selection of an appropriate biopolymeric support, which has various merits including ecologically benign nature, the use of harmless metals, and reproducibility, is the focal point of GC in the 21st century.[51–54] In recent decades, natural polymers have received extensive consideration as outstanding supports for sustainable chemistry[23,46,55–59] since they possess both free amine and OH functional groups simultaneously and are capable of reacting with both nucleophiles and electrophiles through ion pairs and hydrogen bonding.[53,60] Commonly, biopolymers have no destructive impact on the environment as they are biodegradable and obtained from renewable

Department of Chemistry, Pharmaceutical and Heterocyclic Compounds Research Laboratory, Iran University of Science and Technology, Iran. E-mail: mdekamin@iust.ac.ir

† Electronic supplementary information (ESI) available. See DOI: https://doi.org/10.1039/d3na00058c

resources.[61–63] According to the industrial need for clean and green chemical procedures, the use of bio-based heterogeneous catalysts has been increased dramatically.[64–67] Recently, chitosan has been used in different catalytic systems, as a biodegradable and biocompatible natural polymer support,[23,68–76] as well as food and pharmaceutical products.[77] Indeed, ethylenediaminetetraacetic acid (EDTA) has been utilized as an ion exchange and chelating agent for several metal ions in many preceding publications.[78–80] However, this compound has a good capacity to act as a low-cost and nontoxic crosslinker for creating strong bonds with organic compounds having nucleophilic centers.[81–83] Recently, EDTA has been used as a linker to produce different organic or inorganic polymeric supports such as chitosan–EDTA–cellulose network,[84,85] L-asparagine–EDTA–amide silica-coated MNPs, chitosan–EDTA,[86] and diamide–diacid-bridged PMO.[87]

Moreover, asparagine is one of the 20 amino acids found in human cells and it is essential for maintaining balance in the central nervous system.[43] L-Asparagine was the first isolated amino acid from plants about 220 years ago.[88] Its cubic structure was demonstrated as well in 1802.[89] The N : C ratio of 2 : 4 in asparagine made it a good source of nitrogen in living creatures.[90] Due to the presence of acidic and basic sites, abundance in nature, and cost-effectiveness, L-asparagine is a proper candidate, which acts as an available and biocompatible precursor for preparation of simple or complex bifunctional organocatalytic systems.[91,92] On the other hand, according to the literature survey, cinnamic acid (CA) and its derivatives are in the focus of attention of medicine, pharmaceuticals, perfumeries, and cosmetic industries.[93–99] Cinnamic acid derivatives (CADs) are naturally found in fruits, vegetables, and flowers, and CA is an important intermediate for the production of the famous shikimic acid, which is the essential precursor for the synthesis of (−)-oseltamivir (Tamiflu®, an antiviral drug).[100,101] Both acid and ester forms (methyl, ethyl, and benzyl) exist in different essential oils, resins, and balsams. Although there are natural sources for CADs, various chemical and biochemical approaches have been invented for their synthesis including the Perkin reaction,[102] enzymatic method,[103] Knoevenagel condensation accelerated by MW irradiation[104] or promoted by tetraalkylammonium halides,[105] the use of phosphorous oxychloride,[106] or DDQ under ultrasonic conditions,[107] Claisen–Schmidt condensation, and HCR.[108] Among these procedures, green HCR catalyzed by biopolymeric-based catalysts has been performed recently.[61–63] Finally, based on the applicable experiences in our research group in terms of green catalysis and biopolymers, we decided to design novel bio-based catalysts for the HCR. In continuation of our interest to develop novel and

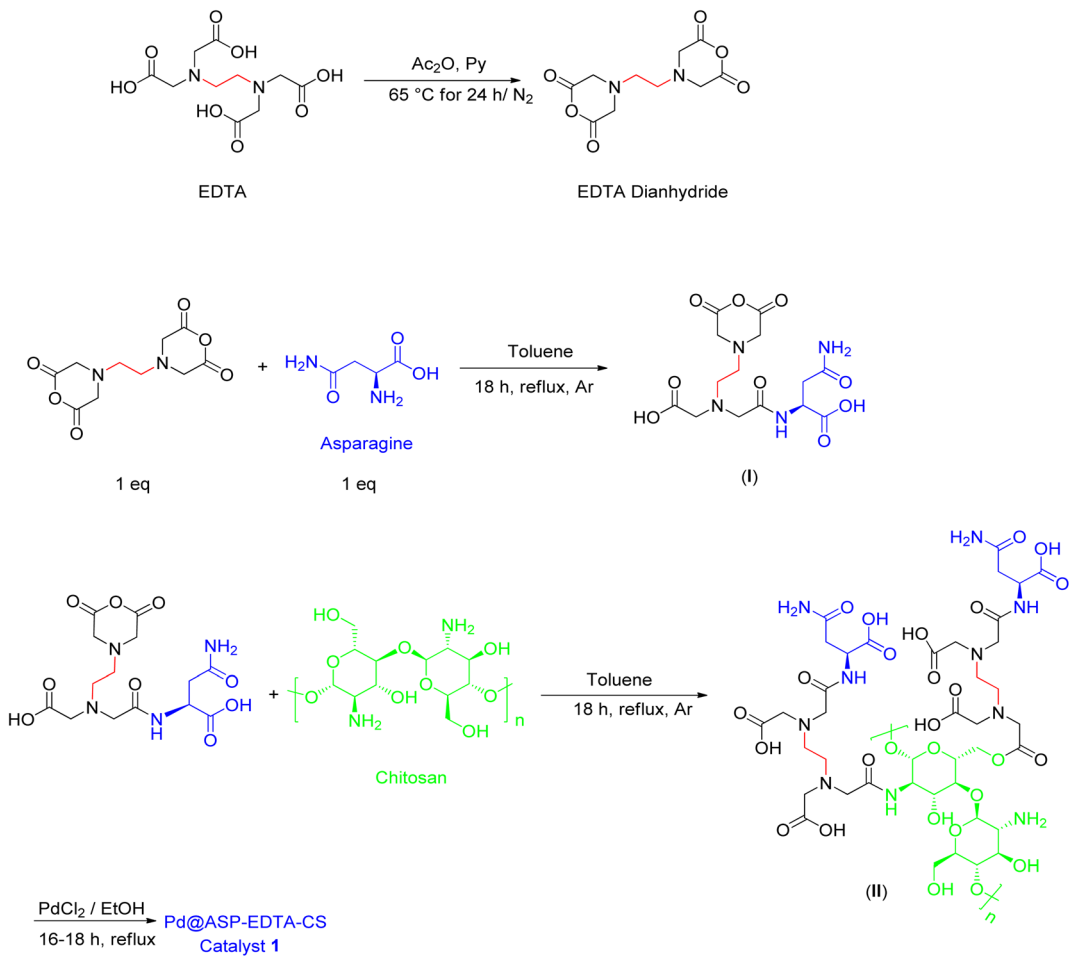

Scheme 1 Schematic representation for the synthesis of Pd@ASP–EDTA–CS nanocatalyst (1).

more efficient supramolecular catalytic systems for different organic transformations,[87,109,110] we herein report the synthesis and characterization of a new Pd(II) supported on the biopolymeric chitosan support. The Pd@ASP–EDTA–CS catalyst was prepared by grafting of L-asparagine using the EDTA dianhydride (EDTADA) onto the chitosan backbone biopolymer, followed by chelation of Pd(II) (Scheme 1). The Pd@ASP–EDTA–CS nanocomposite was investigated to promote and improve HCR efficiently at a lower temperature and shorter reaction time to afford corresponding CADs in good to excellent yields.

2. Experimental

2.1. General information

EDTA (MW = 292.24 g mol^{-1}), and L-asparagine (MW = 132.12 g mol^{-1}) were purchased from Merck and used without further purification. Acrylic acid and the corresponding esters, aryl halides, and $PdCl_2$ were purchased from international chemical companies including Sigma-Aldrich and Sumchun. Chitosan (MW = 190–300 kDa, medium molecular weight, 75–85% deacetylation degree) was obtained from Across Company. Analytical TLC experiments were accomplished using Merck Kieselgel 60 F-254 Al-plates and then visualized by UV light and iodine vapor. An Electrothermal 9100 apparatus was used for measuring the melting points of the products. The functional groups of the samples were identified by FTIR spectroscopy (1720-X PerkinElmer) in the range of 600–4000 cm^{-1} using KBr discs. The morphology of the Pd@ASP–EDTA–CS catalyst was examined by FESEM (KYKY EM8000) and TEM (Philips EM 208S) techniques, and the related elements of the catalyst were demonstrated by SEM mapping. For more consideration, the X-ray diffraction pattern and energy-dispersive X-ray spectroscopy of the catalyst were studied by XRD (Bruker D8, Germany) and EDX (Bruker, Germany) techniques, respectively. The TGA curves of the catalyst were recorded by a Bahr Company STA 504 instrument, while the Brunauer–Emmett–Teller (BET) test was performed by a Micromeritics ASAP 2020. The ^1H NMR spectra of the isolated products were recorded at 500 MHz using a Varian-INOVA spectrometer in DMSO-d_6 at ambient temperature (see ESI†).

2.2. General procedure for the preparation of EDTA dianhydride (EDTADA)

EDTA (10.0 g, 34 mmol), pyridine (16 mL) and acetic anhydride (14 mL) were added into a 100 mL round bottom flask equipped with a condenser and a magnetic stirrer. The reaction was mixed at 65–70 °C for 24 h under N_2 atmosphere. After the completion of the reaction, the resulting product was filtered and washed with acetic anhydride (5.0 mL) and dry diethyl ether (10 mL) to afford a white powder. The final product was dried by a rotary evaporator under vacuum at 40–50 °C until a fine and dry white powder was obtained (yield 90–92%, mp: 189–191 °C) (Scheme 1).[111,112]

2.3. Preparation of L-asparagine–EDTA monoanhydride (ASP–MAEDTA)

The prepared EDTADA (0.256 g, 1 mmol) was added into a two-neck round-bottom flask equipped with a condenser and a magnetic stirrer. Then, 3 mL dry toluene was added under Ar atmosphere. After that, exactly one equivalent of L-asparagine (0.132 g, 1.0 mmol) was gradually added over 60 min to react with only one anhydride functioinal group of the EDTADA. Finally, the mixture was refluxed under continuous stirring for 18 h. The desired intermediate (**I**) was filtered and dried under vacuum at 60 °C to afford a creamy white powder (0.386 g, yield = 98.8%).[84,85]

2.4. Preparation of the L-asparagine–ETDA grafted on chitosan

In a double-neck round-bottom flask containing dry toluene (10 mL), intermediate (**I**) (0.35 g) and chitosan (0.7 g) were added. Then, the mixture was stirred and heated at 60–70 °C under Ar atmosphere for 18 h. After the completion of reaction, the mixture was cooled down to r.t. and the suspension was filtered and dried under vacuum to afford 0.49 g of the desired intermediate (**II**) (Scheme 1).

2.5. Synthesis of the Pd@ASP–EDTA–CS catalyst (1)

$PdCl_2$ (24.5 mg) was added to the mixture of intermediate (**II**) (0.49 g) and EtOH (3.0 mL), and the suspension was refluxed for 18 h. After cooling of the mixture to ambient temperature, the prepared catalyst (**I**) was filtered and washed under vacuum with EtOH and then dried in an oven at 70 °C to afford the final catalyst (0.35 g) (Scheme 1).

2.6. General procedure for the synthesis of cinnamic acid derivatives in the HCR catalyzed by Pd@ASP–EDTA–CS catalyst (1)

A mixture of aryl halides (**3a–e**, 2.0 mmol), active alkenes (**4a–d**, 3.0 mmol), potassium carbonate (2.0 mmol) and catalyst **1** (4.0 mg) were added into a three-neck round-bottom flask containing a proper solvent, DMF or CH_3CN (3.0 mL), followed by heating and stirring for an appropriate time under Ar atmosphere, as designated in Table 2. After the completion of the reaction, as monitored by TLC [eluent *n*-hexane : EtOAc = 5 : 1], and cooling the reaction mixture to r.t., the catalyst **1** was filtered. Then, the solvent was recovered under reduced pressure, and a mixture of $CHCl_3$ (5 mL) and water (5 mL) was added to the reaction flask followed by stirring for 30 min. Next, the mixture was transferred to a decanter and settled for 0.5 h. The mixture was decanted to separate the undesired salts and materials. Afterward, the water content of the organic layer was removed by utilizing dry Na_2SO_4. After that, the organic phase was recycled under vacuum to afford the final products. Finally, the crude product was recrystallized from EtOH to obtain the pure corresponding product (see ESI†).

2.7. Spectral data of the selected products

2.7.1. Cinnamic acid (5a). White crystals, m.p. = 132–133 °C; FTIR (KBr, cm^{-1}) ν = 3450, 2928, 1694, 1670, 1562, 1441, 1096; ^1H NMR (500 MHz, DMSO-d_6) δ (ppm) = 12.40 (S, 1H), 7.59 (d, J = 16.0 Hz, 1H), 7.71–7.63 (m, 2H), 7.44–7.32 (m, 3H), 6.52 (d, J = 16.0 Hz, 1H).

3. Results and discussion

3.1. Characterization of Pd@ASP–EDTA–CS nanocatalyst (1)

The overall procedure for the synthesis of Pd@ASP–EDTA–CS catalyst (**1**) has been summarized in Scheme 1. The catalyst was characterized using different spectroscopic, microscopic and analytical techniques including Fourier transform infrared (FTIR) spectroscopy, energy-dispersive X-ray (EDX) spectroscopy, field emission scanning electron microscopy (FESEM), X-ray powder diffraction (XRD), thermogravimetric analysis (TGA), Brunauer–Emmett–Teller (BET) surface area analysis, and differential reflectance spectroscopy (DRS).

3.1.1. Fourier transform infrared (FTIR) analysis. FTIR spectroscopy was employed to determine the functional groups and structure of EDTADA (a), L-asparagine (b) chitosan (c), and the Pd@ASP–EDTA–CS catalyst (**1**). The results are illustrated in the overlay spectra in Fig. 1. In the FTIR spectra, the observed bands at 3400–3600 are attributed to the hydroxyl and amine groups, and the vibration double bands of the C=O groups in EDTA dianhydride stands at 1810 and 1760, respectively, which is displaced by amidic and acidic groups at 1675 cm^{-1} and 1733 cm^{-1}, respectively. The sp^3 C–H bands are shown at 2900–3000 cm^{-1}, and the absorbance bands at 1200–1400 cm^{-1} are assigned to the bending of –NH groups. The C–O stretching bands are located at about 1100 cm^{-1}.

3.1.2. Energy dispersive X-ray spectroscopy (EDX) analysis. Chemical composition and elemental analysis of the Pd@ASP–

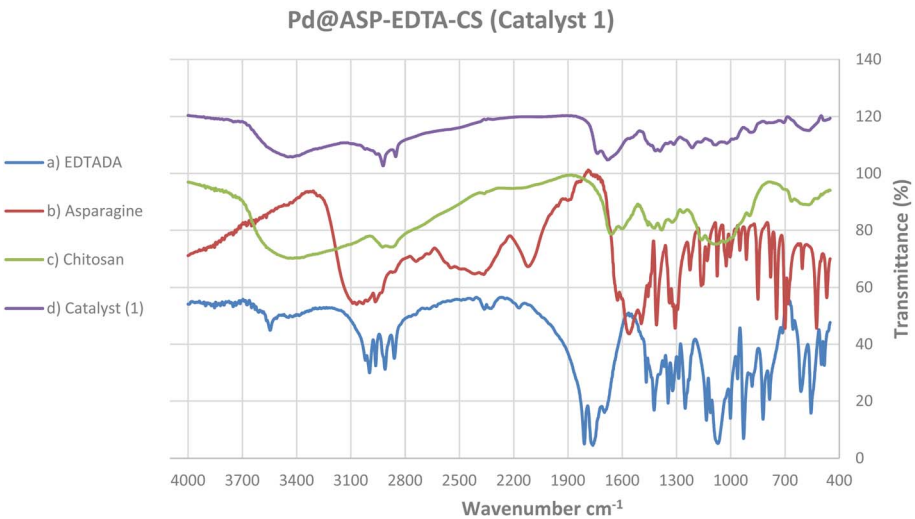

Fig. 1 FTIR spectra of the Pd@ASP–EDTA–CS catalyst (**1**).

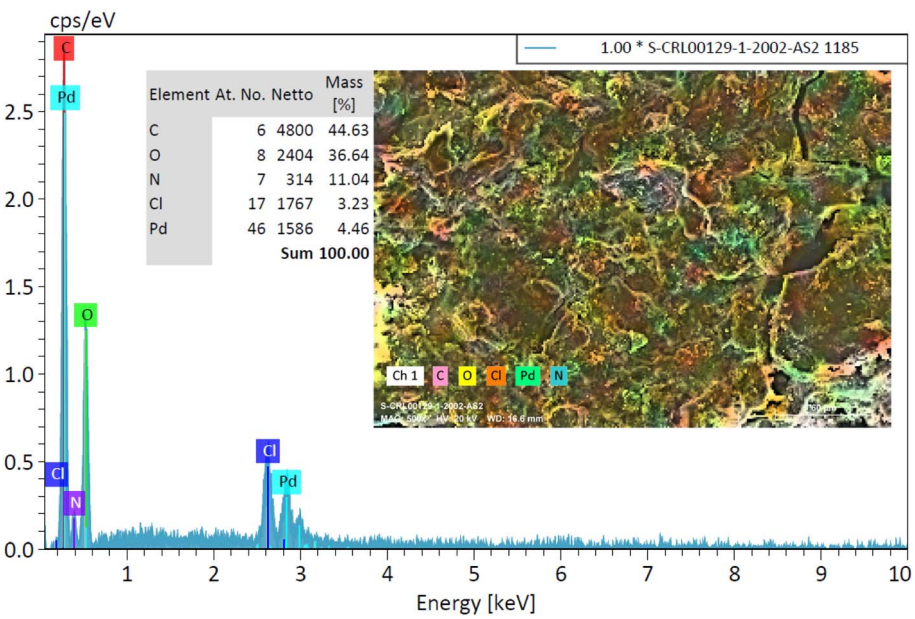

Fig. 2 EDS spectrum of the Pd@ASP–EDTA–CS nanocatalyst (**1**).

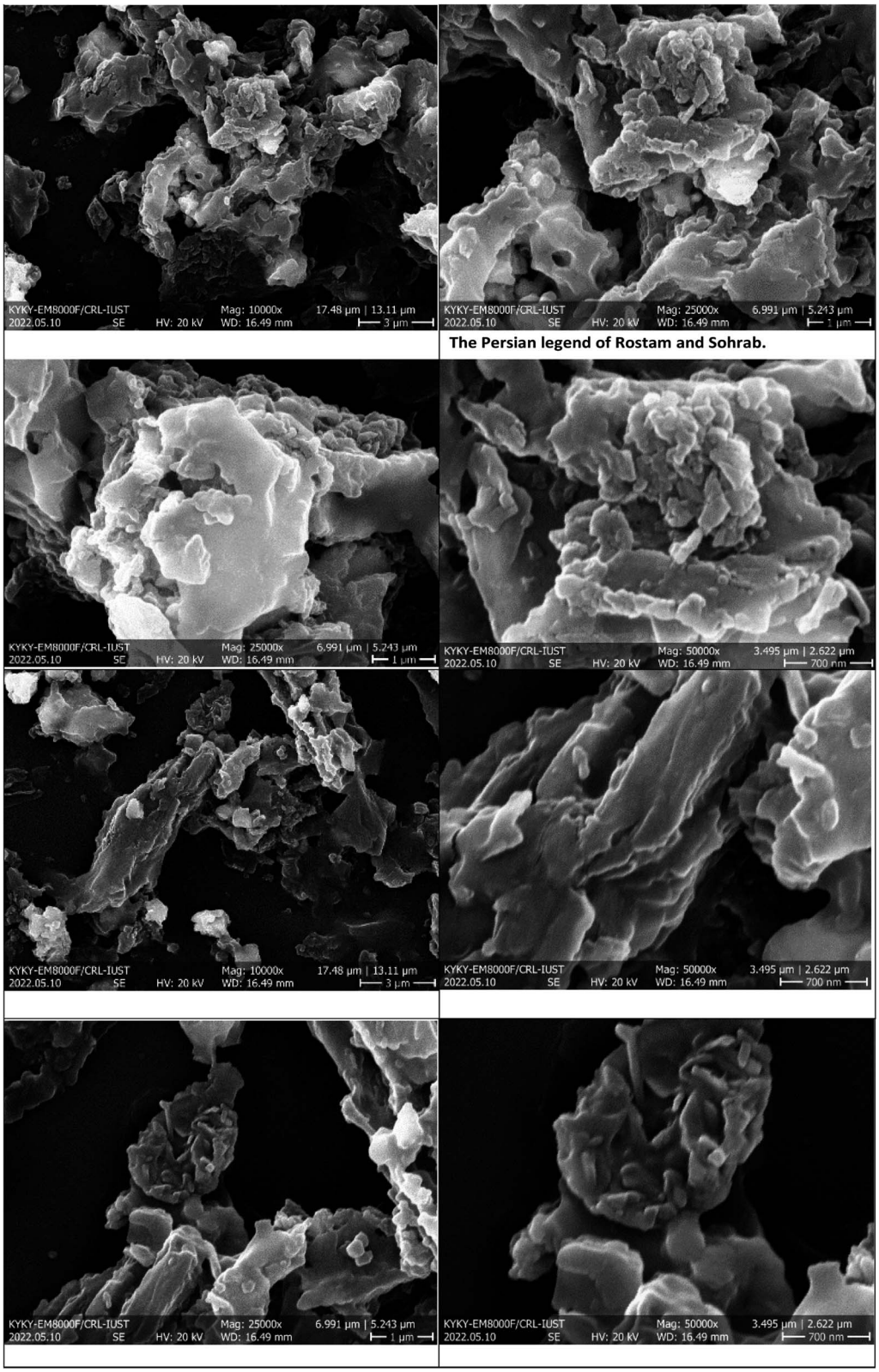

Fig. 3 FESEM images of the Pd@ASP–EDTA–CS nanocatalyst (**1**).

EDTA–CS (**1**) was carried out using energy-dispersive X-ray spectroscopy (EDX). The EDX spectrum of the catalyst is depicted in Fig. 2. In addition, the EDX analysis showed the well-defined peaks related to C, O, N, Cl, and Pd in the structure of Pd@ASP–EDTA–CS (**1**) with the percentages of 44.63, 36.64, 11.04, 3.23, and 4.46, respectively.

3.1.3. Field emmision scanning electron microscopy (FESEM) analysis. The morphology and texture of the Pd@ASP–

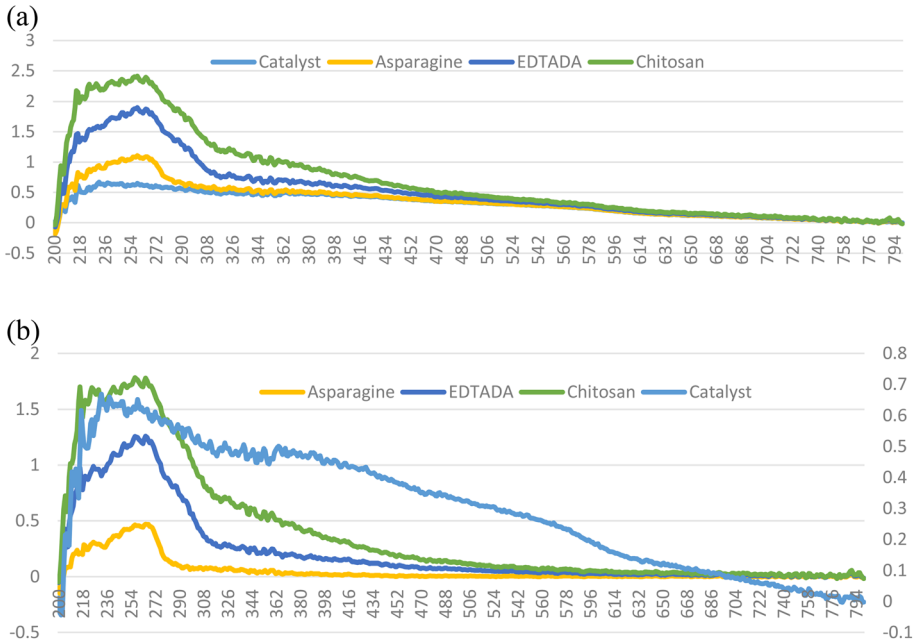

Fig. 4 (a) DRS of the Pd@ASP–EDTA–CS catalyst (**1**) and its components. (b) Intensified DRS of Pd@ASP–EDTA–CS catalyst (**1**).

EDTA–CS (**1**) were specified by FESEM analysis, and the related photographs are presented in Fig. 3. According to these FESEM photographs, the size and surface shape of the catalyst are well observed, which proves that the particles have special layered morphology, the mythological figure of the Persian legend of Rostam and Sohrab, which shows the black and white combat from the top view in the first image with defined pores and without agglomeration.

3.1.4. Differential reflectance spectroscopy (DRS) of the catalyst (1) and its components. By comparing the DRS of the catalyst (**1**) and its components, it can be implied that the structure of the catalyst consists of bands, which are found in the precursors (Fig. 4a). Through more investigation, by carrying out the Excel adjustments on the secondary axis for the catalyst, more obvious points of the combination are shown (Fig. 4b).

3.1.5. X-ray diffraction (XRD) analysis of the catalyst (1). The XRD pattern of Pd@ASP–EDTA–CS (**1**) is shown in (Fig. 5). The observed peaks were compared with the standard reference patterns of EDTA (card no. JCPDS, 00-033-1672), chitosan (card

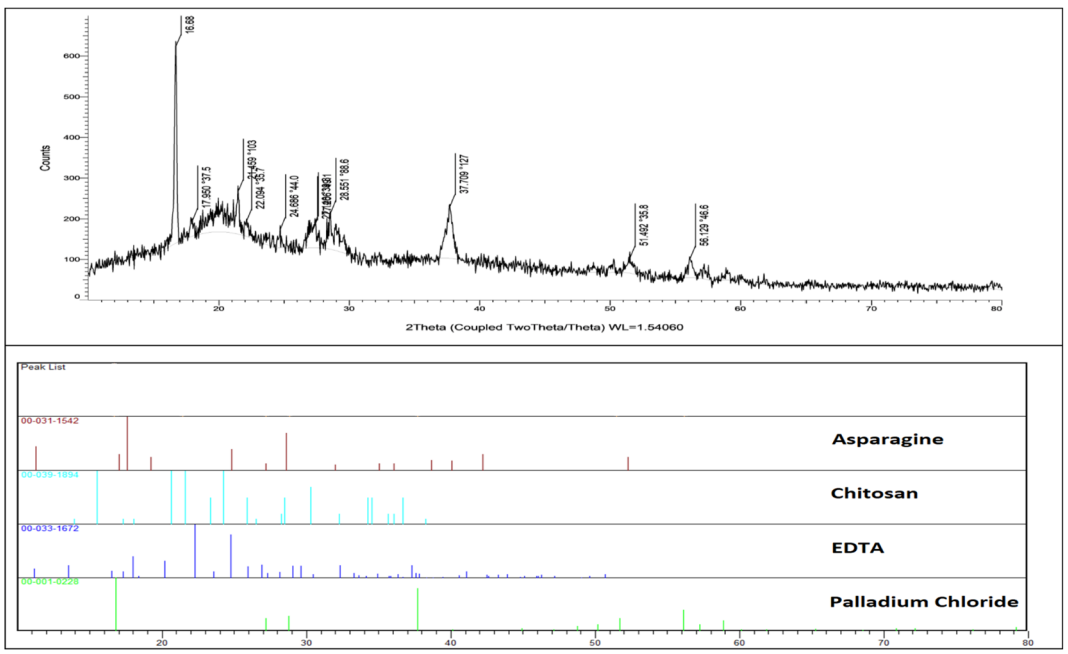

Fig. 5 XRD pattern of the Pd@ASP–EDTA–CS catalyst (**1**).

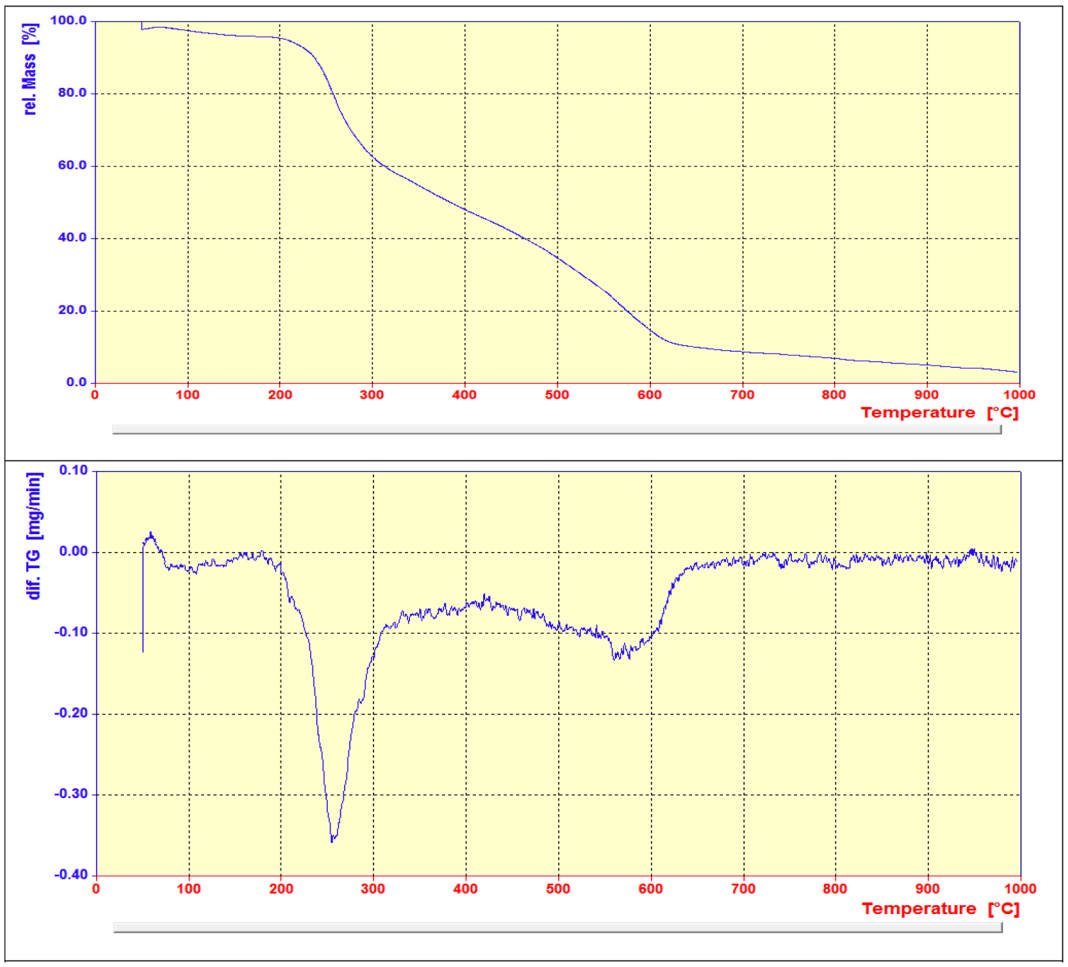

Fig. 6 (a) TGA and (b) DTA curves of the Pd@ASP–EDTA–CS catalyst (**1**).

no. JCPDS, 00-039-1834), L-asparagine (card no. JCPDS, 00-031-1542), and $PdCl_2$ (card no. JCPDS, 00-001-0228). The sharp peaks in the pattern demonstrate the presence of crystalline regions in the structure of catalyst **1** as well as the combination of several peaks after the grafting of L-asparagine onto the chitosan backbone by the EDTA linker and subsequent chelation of Pd(II).

3.1.6. Thermogravimetric analysis (TGA) and BET of the catalyst (1). The thermal stability of Pd@ASP–EDTA–CS

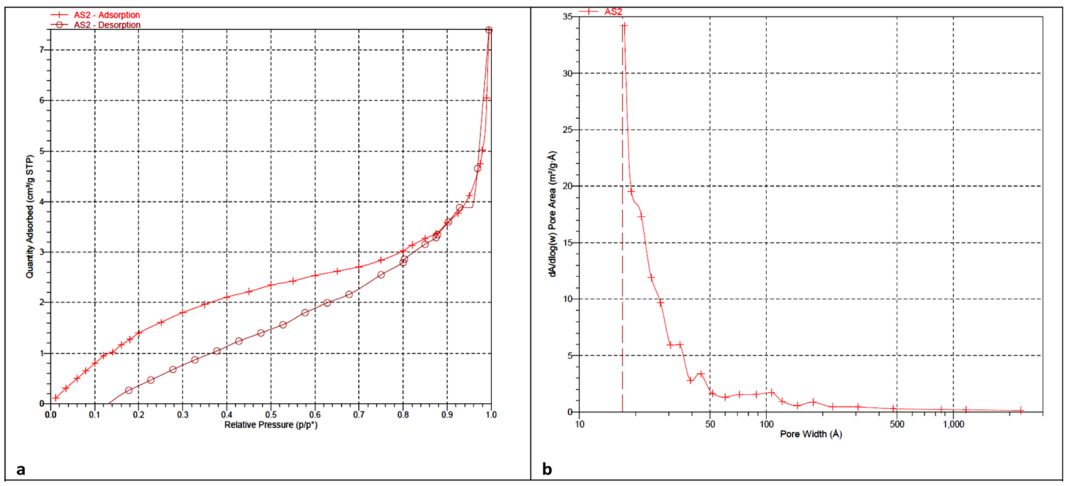

Fig. 7 (a) The N_2 adsorption–desorption isotherm of the Pd@ASP–EDTA–CS catalyst (**1**) and (b) the pore width of the Pd@ASP–EDTA–CS catalyst (**1**).

nanocomposite (**1**) was investigated under air atmosphere in the temperature range of 50–1000 °C (Fig. 6a). The initial mass loss for the catalyst **1** are about 3 wt% (below 100 °C) and 40 wt% (at about 200–330 °C), which represent the removal of water or organic solvents and degradation of peripheral L-asparagine moieties, respectively. The catalyst (**1**) displays another stage for mass loss over the temperature range of TGA, and the total weight loss of the catalyst reaches about 85%, which clearly demonstrates the effect of organic units grafted onto the surface of chitosan chains. The stability of the catalyst is about 200 °C (Fig. 6b). After the first two steps, including the removal of water or organic solvents and the degradation of the L-asparagine moieties, the high weight loss (about 45%) at 330–650 °C can be attributed to the decomposition of the EDTA and chitosan moieties that remain in the catalyst structure. These results also indicate that EDTA and L-asparagine have been successfully grafted onto the chitosan polymeric surface. The effect of chelated Pd nanoparticles on the biopolymeric support caused an increase in the thermal stability of the catalyst in comparison to the pristine chitosan, as seen from the TGA results.[113]

In addition, the porosity of the Pd@ASP–EDTA–CS catalyst (**1**) was examined through the physisorption of N_2 at 77 K. The illustrative curve of the catalyst displays a type III nitrogen gas sorption isotherm, which indicates that there are plentiful microspores in the supramolecular biopolymeric-based catalyst **1**. The results demonstrated that the specific surface area of catalyst **1** is 9.1004 $m^2\ g^{-1}$. The BJH adsorption cumulative volume of the pores between 17.000 Å and 3000.000 Å width was 0.011020 $cm^3\ g^{-1}$, the BJH adsorption average pore width (4*V*/*A*) was 73.681 Å, the BJH desorption average pore width (4*V*/*A*) was 95.458 Å, and the adsorption average pore width (4*V*/*A* by BET) was 18.4597 Å. The N_2 adsorption–desorption isotherm and BJH pore volume of the catalyst are shown in Fig. 7a and b.

3.2. Optimization of conditions in the HCR reaction using Pd@ASP–EDTA–CS catalyst (1)

In our preliminary experiments, the catalytic activity of the as-prepared catalyst **1** was evaluated in the synthesis of cinnamic acid derivatives (**5**) through the Heck cross-coupling reaction between different halobenzenes and various active alkenes. For this purpose, the reaction conditions were optimized using certain mixtures of iodobenzene (**3a**, 2.0 mmol), methyl acrylate (**4b**, 3.0 mmol), and K_2CO_3 (2.0 mmol) as the model reaction. In a systematic screening, the reaction conditions were investigated precisely by considering several crucial variables such as catalyst loading, reaction time, solvent, and reaction temperature, as given in Table 1. Primarily, in the absence of any catalyst, the progress of the model reaction even after a long reaction time at r.t. or under reflux conditions was not detected (entries 1, 2). On the other hand, no detectable yield for the model reaction in the presence of Pd@ASP–EDTA–CS catalyst (**1**) without using K_2CO_3 base was obsereved (entries 3, 4). A trace amount of the desired product, methyl cinnamate (**5b**), was obtained by simultaneous using of the catalyst **1** and K_2CO_3 under solvent-free conditions (entry 5). Interestingly, when the catalyst and base in proper solvents such as DMF and CH_3CN were used the best yeilds of the desired product were obtained (entries 6, 7). On the other hand, the model reaction in toluene afforded only a trace amount of the desired product

Table 1 Optimization of the conditions for HCR in the model reaction of iodobenzene (**3a**) and methyl acrylate (**4b**) to afford methyl cinnamate (**5b**) under different conditions in the presence of Pd@ASP–EDTA–CS catalyst (**1**)[a]

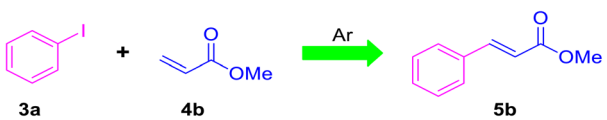

3a **4b** **5b**

Entry	Catalyst	Base	Solvent	Temp. (°C)	Time (h)	Yield[b] (%)
1	—	K_2CO_3	DMF	r.t	48	N.R
2	—	K_2CO_3	DMF	Reflux	48	N.R
3	Pd@ASP–ETDA–CS	—	DMF	Reflux	48	N.R
4	Pd@ASP–ETDA–CS	—	CH_3CN	Reflux	48	N.R
5	Pd@ASP–ETDA–CS	—	Solvent-free	80	24	Trace
6	Pd@ASP–ETDA–CS	K_2CO_3	**DMF**	**90**	**14–20**	**78–90**
7	Pd@ASP–ETDA–CS	K_2CO_3	**CH_3CN**	**80**	**16–20**	**75–90**
8	Pd@ASP–ETDA–CS	K_2CO_3	Toluene	105	36	Trace
9	Pd@ASP–ETDA–CS	K_2CO_3	H_2O	105	36	Trace
10	ASP–ETDA	K_2CO_3	DMF	130	36	N.R
11	ASP–ETDA–CS	K_2CO_3	DMF	130	36	N.R
12	ASP–ETDA	K_2CO_3	CH_3CN	80	36	N.R
13	ASP–ETDA–CS	K_2CO_3	CH_3CN	80	36	N.R
14	L-Asparagine	K_2CO_3	DMF	130	36	N.R
15	EDTA	K_2CO_3	DMF	130	36	N.R

[a] Reaction conditions: aryl halide (**3a**, 2.0 mmol), alkene (**4b**, 3.0 mmol), K_2CO_3 (2.0 mmol), Pd@ASP–EDTA–CS (**1**, 4.0 mg), and solvent (3.0 mL) unless otherwise stated. [b] Isolated yield.

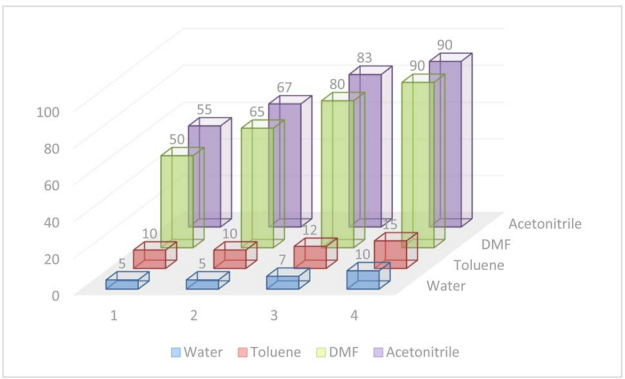

Fig. 8 Investigation of the optimized loading of the Pd@ASP–EDTA–CS catalyst (**1**) in different solvents for HCR to afford **5b**.

(entry 8). The same result was acquired for H_2O (entry 9). Furthermore, the model reactions in the presence of EDTA, L-asparagine, EDTA–ASP, and the support (ASP–EDTA–CS) were separately investigated without using any Pd(II) species, but there were no yields of the desired product **5b** (entries 10–15). While the catalyst amount used in these experiments was just 4.0 mg, other quantities less than 4.0 mg afforded lower reaction yields. Indeed, the utilized catalytic amount was dramatically lower than that of optimized conditions since the quantity of loaded $PdCl_2$ on the catalyst **1** was 4.46%. Therefore, the total employed Pd, as an expensive metal, based on the mass of aryl halides was about 0.1%.

According to the optimization experiments for the model reaction, the impact of various solvents and the amount of utilized catalyst on the yield of desired product **5b** is illustrated

Table 2 Synthesis of different derivatives of cinnamic acid (**5a–l**) through HCR catalyzed by the Pd@ASP–EDTA–CS catalyst (**1**) under the optimized conditions[a]

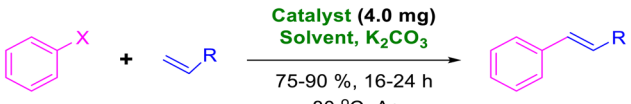

Entry	Ar–X	Alkene	Product	Time (h)	Temp. (°C)	Yield[b] (%)	m.p. (°C)	m.p. (°C) (Lit.)
1	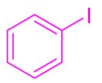 **3a**	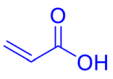 **4a**	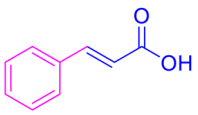 **5a**	14	80	85	131–132	133 (ref. 120)
2	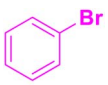 **3b**	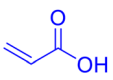 **4a**	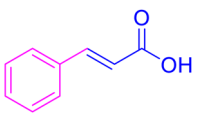 **5a**	20	80	75	131–132	133
3	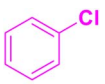 **3c**	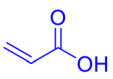 **4a**	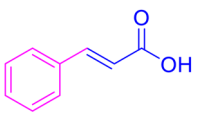 **5a**	40	80	20	—	133
4	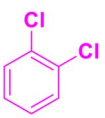 **3d**	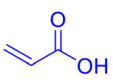 **4a**	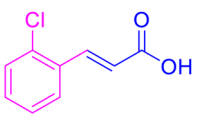 **5e**	48	80	Trace	—	212
5	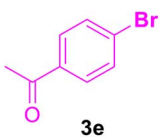 **3e**	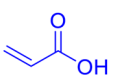 **4a**	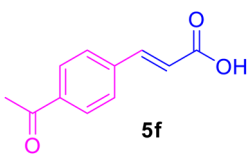 **5f**	48	80	Trace	—	224–226 (ref. 121)
6	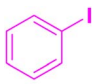 **3a**	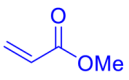 **4b**	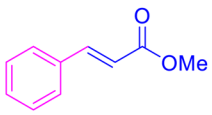 **5b**	17	80	90	33–35	34–38 (ref. 122)

Table 2 (*Contd.*)

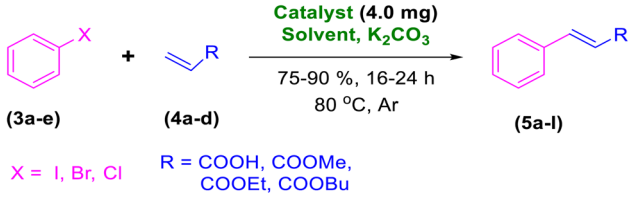

Entry	Ar–X	Alkene	Product	Time (h)	Temp. (°C)	Yield[b] (%)	m.p. (°C)	m.p. (°C) (Lit.)
7	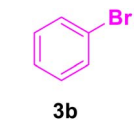 3b	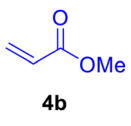 4b	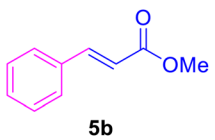 5b	19	80	80	33–35	34–38
8	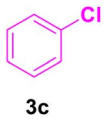 3c	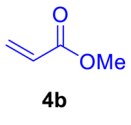 4b	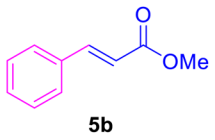 5b	36	80	20	33–35	34–38
9	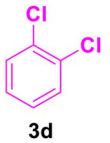 3d	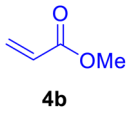 4b	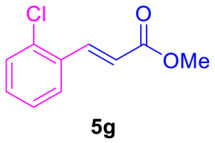 5g	48	80	Trace	—	34–38
10	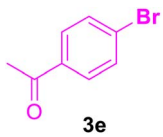 3e	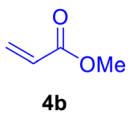 4b	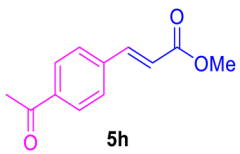 5h	48	80	Trace	—	34–38
11	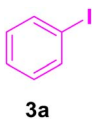 3a	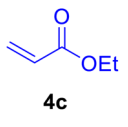 4c	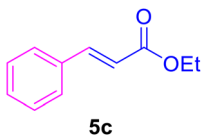 5c	14	80	85	Liquid	(6.5–7.5)[123]
12	 3b	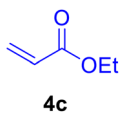 4c	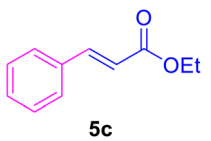 5c	20	80	76	Liquid	6.5–7.5
13	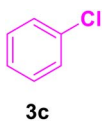 3c	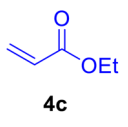 4c	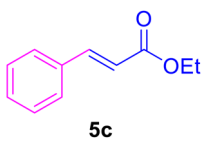 5c	36	80	20	Liquid	6.5–7.5
14	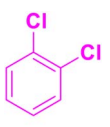 3d	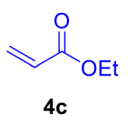 4c	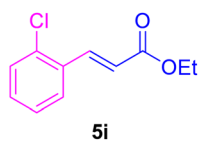 5i	48	80	Trace	—	—
15	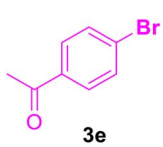 3e	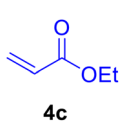 4c	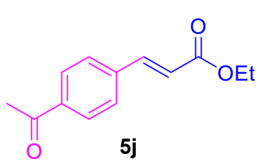 5j	48	80	Trace	—	—

Table 2 (*Contd.*)

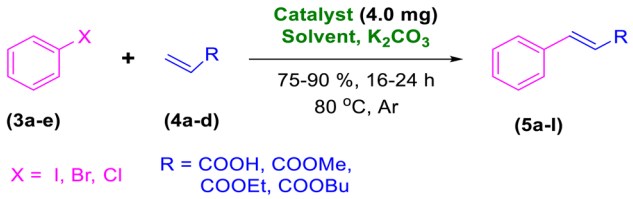

Entry	Ar–X	Alkene	Product	Time (h)	Temp. (°C)	Yield[b] (%)	m.p. (°C)	m.p. (°C) (Lit.)
16	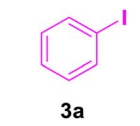 3a	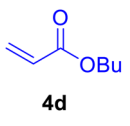 4d	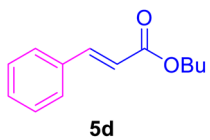 5d	16	80	85	Liquid[99]	B.P.: 271
17	 3b	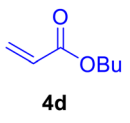 4d	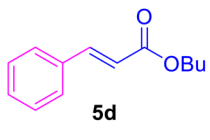 5d	20	80	80	Liquid	B.P.: 271
18	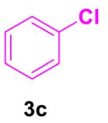 3c	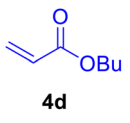 4d	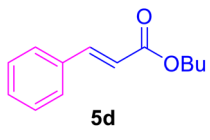 5d	36	80	20	Liquid	B.P.: 271
19	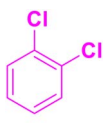 3d	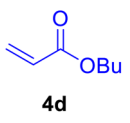 4d	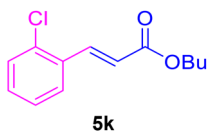 5k	48	80	Trace	—	—
20	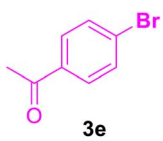 3e	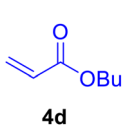 4d	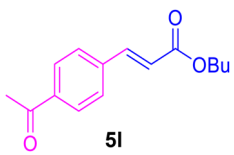 5l	48	80	Trace	—	—

[a] Reaction conditions: aryl halide (**3a–e**, 2.0 mmol), alkene (**4a–d**, 3.0 mmol), K_2CO_3 (2.0 mmol), Pd@ASP–EDTA–CS (**1**, 4.0 mg), and solvent (3.0 mL). [b] Isolated yield.

in Fig. 8. The model reaction was investigated in different solvents such as CH_3CN, toluene, water, and DMF using catalyst (**1**) with different loadings (in mg). Based on the obtained results summarized in Table 1 and Fig. 8, the optimum reaction conditions were found to be 4.0 mg catalyst loading in DMF or CH_3CN solvents at 80–90 °C.

After the abovementioned experimetns, the scope of the reaction was expanded using aryl halides having electron-withdrawing groups (EWG) under the optimized conditions. The results are summarized in Table 2. As expected, by using this novel heterogeneous catalytic system, the obtained yields for aryl halides containing EWG were poor (entries 4, 5, 9, 10, 14, 15, 19 and 20).

3.3. The proposed mechanism for the synthesis of cinnamic acid derivatives in the presence of catalyst 1

According to the XRD pattern, the oxidation state of palladium in the Pd@ASP–EDTA–CS catalyst (**1**) is (II). Moreover, the active catalytic sites in HCR generally contain Pd(0) species. Therefore, the reduction of Pd(II) in catalyst **1** to its activated form, Pd(0), occurs smoothly in DMF and CH_3CN as oxidizable solvents.[114–116] Hence, the oxidative addition of the Pd(0) species to aryl halide **3a–e** affords intermediate (**I**), and then coordination insertion between intermediate (**I**) and alkene **4a–d** gives intermediate (**II**). Afterward, the migratory insertion of hydrogen, followed by C–C bond rotation, generates intermediate (**III**), which produces the desired product **5a–l** and intermediate (**IV**) through *syn*-β-hydride elimination. Finally, the activated form of the catalyst **1** is recovered by the reductive elimination of HI using K_2CO_3 base (Scheme 2).[117–119]

3.4. Reusability of the Pd@ASP–EDTA–CS catalyst (1)

One of the vital parameters in heterogeneous catalytic processes is the reusability of catalyst. For the evaluation of this parameter, the model reaction was examined using the recycled

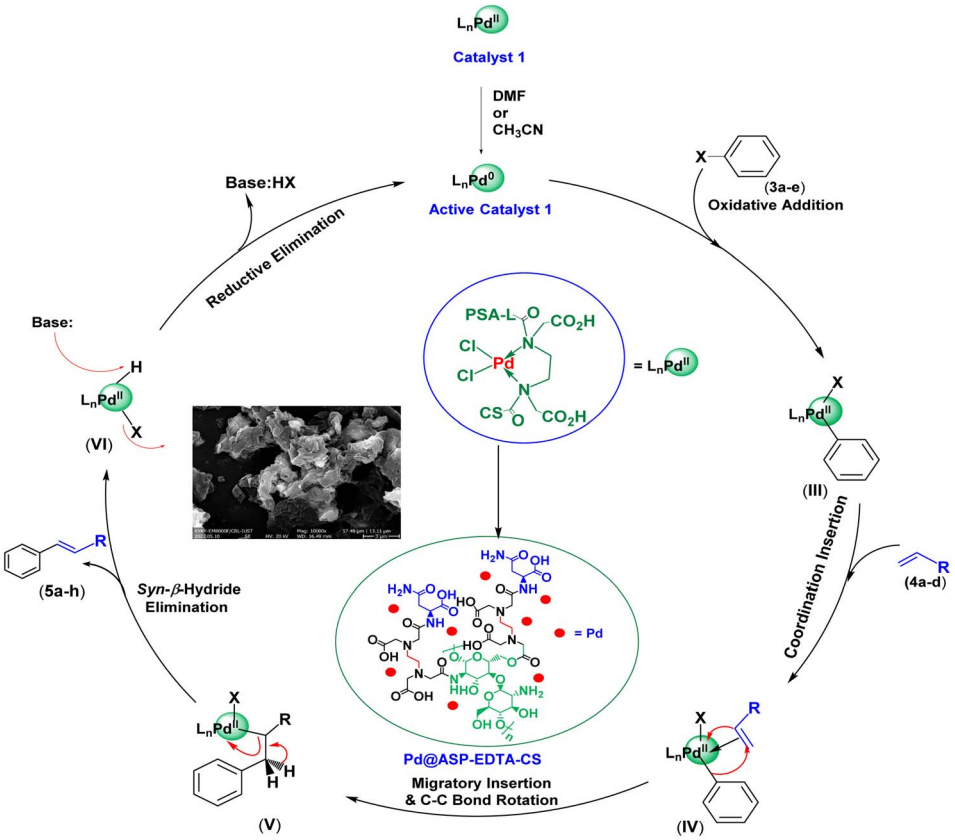

Scheme 2 The proposed mechanism for the synthesis of cinnamic acid derivatives **5** using aryl halides and active alkenes in the presence of catalyst **1**.

catalyst for five consecutive runs. At the end of each run, the utilized catalyst **1** was removed by a simple filtration, followed by washing with EtOH, drying at 70 °C, and reused in the next model reaction. The obtained results are summarized in Fig. 9. Considering the results of isolated yields for the model reaction, the catalytic activity of the catalyst after five runs shows a slight decrease, which exhibits the proper conservation of the catalytic activity after recycling.

3.5. Leaching test of Pd in the reaction medium (hot filtration test)

Finally, to check the leaching of Pd(0) species into the reaction medium, the model Heck reaction was heated, and the catalyst **1** was removed from the hot reaction mixture after 3 h by filtration. After that, the reaction continued without any catalyst. Although the reaction mixture was heated under

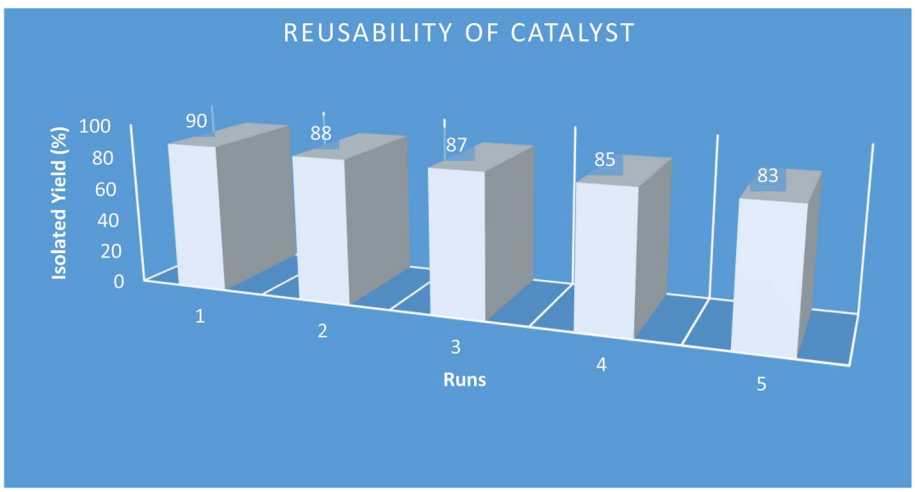

Fig. 9 Reusability of the catalyst **1** in the model reaction to afford methyl cinnamate (**5b**).

Table 3 The comparison of the obtained results for the HCR using catalyst **1** and other catalytic systems

Entry	Catalyst	Reaction conditions	Catalyst amount	Time (h)	Yield (%)	Reference
1	Trifunctional *N*,*N*,*O*-terdentate amido/pyridyl carboxylate Pd(II) complexes	DMF/145 °C/base	0.01 mol%	20	3–92	124
2	Trifunctional *N*,*N*,*O*-terdentate amido/pyridyl carboxylate Pd(II) complexes	DMF/145 °C/Na_2CO_3	0.01 mol%	20	92	124
3	$Pd(OAc)_2$	NMP/135 °C/NaOAc//UV-VIS	0.05 mol%	44	80	125
4	CMH–Pd(0)	DMF/120 °C/Et_3N	50 mg	6	90	126
5	NHC–Pd/IL@SiO_2	NMP/140 °C/NaOAc	0.01 mol%	24	94	127
6	Pd(quinoline-8-carboxylate)$_2$	DMF/130 °C/K_2CO_3	0.01 mol%	30	39–94	128
7	OCMCS–Pd	DMF/140 °C/Et_3N	0.02 mmol	12	89–98	129
8	**Pd@ASP–EDTA–CS**	DMF/90 °C/K_2CO_3	**4.0 mg**	**16**	**90**	**This work**
9	**Pd@ASP–EDTA–CS**	CH_3CN/80 °C/K_2CO_3	**4.0 mg**	**18**	**90**	**This work**

the optimized conditions for about 36 h, the progress stopped at the previous level and the reaction did not proceed on increasing the reaction time either. These findings confirmed the heterogeneous nature of the catalyst **1** as there was no leaching of Pd or observing re-precipitation of the catalyst.

3.6. Comparison of the catalytic activity of the Pd@ASP–EDTA–CS catalyst (1) with other catalytic systems

In order to compare the efficacy of Pd@ASP–EDTA–CS catalyst (**1**) with other catalytic systems for the application in the HCR, several parameters including the catalyst loading as well as reaction conditions, required time, and yield of the desired product **5b** were taken into consideration and the results are summarized in Table 3. It can be seen that Pd@ASP–EDTA–CS heterogeneous catalyst (**1**) shows higher efficiency than previously reported catalytic systems for the HCR.

4. Conclusion

In summary, a novel and thermally stable green heterogeneous supramolecular catalytic system has been introduced using both chitosan and L-asparagine amino acid, as naturally-occurring resources, grafted by EDTA to produce a natural bio-based support for chelation of Pd(II) species onto the backbone of the modified chitosan with high dispersion. In covering the green metrics, the quantity of catalyst **1**, compared to other HCRs, was very competitive and cost-effective. On the other hand, the complete recovery of organic solvents has lessened the related impact on the environment. The catalyst demonstrated a highly efficient, easy, and sustainable application in the HCR, and the final yields were good to excellent. The recovery of the catalyst was performed by easy filtration at the end of the reaction cycles, and the catalytic activity showed only a slight decrease after five consecutive reaction runs without the leaching of the Pd species in the reaction medium and also the final products. Hence, the abovementioned advantages of the catalyst make it a suitable candidate for the pharmaceutical and fine chemicals industrial sectors.

Author contributions

Mohammad Dohendou: methodology, investigation, writing – original draft & editing, formal analysis, data curation; Mohammad G. Dekamin: conceptualization, funding acquisition; supervision, project administration; resources; writing – review & editing, resources; Danial Namaki: methodology, investigation, data curation.

Conflicts of interest

There are no conflicts to declare.

Acknowledgements

We are grateful for the financial support from The Research Council of Iran University of Science and Technology (IUST), Tehran, Iran (Grant No. 160/22061). We would also like to acknowledge the support of the Iran Nanotechnology Initiative Council (INIC).

Notes and references

1 T. Mizoroki, K. Mori and A. Ozaki, Arylation of olefin with aryl iodide catalyzed by palladium, *Bull. Chem. Soc. Jpn.*, 1971, **44**(2), 581.
2 R. F. Heck and J. Nolley Jr, Palladium-catalyzed vinylic hydrogen substitution reactions with aryl, benzyl, and styryl halides, *J. Org. Chem.*, 1972, **37**(14), 2320–2322.
3 C. G. Na, S. H. Kang and R. Sarpong, Development of a C–C Bond Cleavage/Vinylation/Mizoroki–Heck Cascade Reaction: Application to the Total Synthesis of 14-and 15-Hydroxypatchoulol, *J. Am. Chem. Soc.*, 2022, **144**(42), 19253–19257.
4 N. A. Stini, P. L. Gkizis and C. G. Kokotos, Cyrene: A Bio-based Solvent for the Mizoroki-Heck Reaction of Aryl Iodides, *Org. Biomol. Chem.*, 2023, **21**, 351–358.
5 S. Wang, M. Yuan, Q. Zhang and S. Huang, Recent progress in copper nanocatalysis for sustainable transformations, *Curr. Opin. Green Sustainable Chem.*, 2022, 100698.

6 C.-J. Li and P. T. Anastas, Green Chemistry: present and future, *Chem. Soc. Rev.*, 2012, **41**(4), 1413–1414.
7 R. A. Sheldon, Metrics of green chemistry and sustainability: past, present, and future, *ACS Sustainable Chem. Eng.*, 2018, **6**(1), 32–48.
8 H. C. Erythropel, J. B. Zimmerman, T. M. de Winter, L. Petitjean, F. Melnikov, C. H. Lam, A. W. Lounsbury, K. E. Mellor, N. Z. Janković and Q. Tu, The Green ChemisTREE: 20 years after taking root with the 12 principles, *Green Chem.*, 2018, **20**(9), 1929–1961.
9 K. N. Ganesh, D. Zhang, S. J. Miller, K. Rossen, P. J. Chirik, M. C. Kozlowski, J. B. Zimmerman, B. W. Brooks, P. E. Savage, D. T. Allen and A. M. Voutchkova-Kostal, Green Chemistry: A Framework for a Sustainable Future, *Org. Process Res. Dev.*, 2021, **25**(7), 1455–1459.
10 J. Terao, H. Watanabe, A. Ikumi, H. Kuniyasu and N. Kambe, Nickel-Catalyzed Cross-Coupling Reaction of Grignard Reagents with Alkyl Halides and Tosylates: Remarkable Effect of 1,3-Butadienes, *J. Am. Chem. Soc.*, 2002, **124**(16), 4222–4223.
11 T. M. Gøgsig, J. Kleimark, S. O. Nilsson Lill, S. Korsager, A. T. Lindhardt, P.-O. Norrby and T. Skrydstrup, Mild and Efficient Nickel-Catalyzed Heck Reactions with Electron-Rich Olefins, *J. Am. Chem. Soc.*, 2012, **134**(1), 443–452.
12 N. Paul, T. Patra and D. Maiti, Recent Developments in Hydrodecyanation and Decyanative Functionalization Reactions, *Asian J. Org. Chem.*, 2022, **11**(1), e202100591.
13 K. Juhász, Á. Magyar and Z. Hell, Transition-Metal-Catalyzed Cross-Coupling Reactions of Grignard Reagents, *Synthesis*, 2021, **53**(06), 983–1002.
14 Y. Zhu, W. Dong and W. Tang, Palladium-catalyzed cross-couplings in the synthesis of agrochemicals, *Adv. Agrochem*, 2022, **1**, 125–138.
15 M. Farhang, A. R. Akbarzadeh, M. Rabbani and A. M. Ghadiri, A retrospective-prospective review of Suzuki–Miyaura reaction: From cross-coupling reaction to pharmaceutical industry applications, *Polyhedron*, 2022, 116124.
16 J. Magano and J. R. Dunetz, Large-scale applications of transition metal-catalyzed couplings for the synthesis of pharmaceuticals, *Chem. Rev.*, 2011, **111**(3), 2177–2250.
17 C. Torborg and M. Beller, Recent applications of palladium-catalyzed coupling reactions in the pharmaceutical, agrochemical, and fine chemical industries, *Adv. Synth. Catal.*, 2009, **351**(18), 3027–3043.
18 S. Sobhani, H. Hosseini Moghadam, J. Skibsted and J. M. Sansano, A hydrophilic heterogeneous cobalt catalyst for fluoride-free Hiyama, Suzuki, Heck and Hirao cross-coupling reactions in water, *Green Chem.*, 2020, **22**(4), 1353–1365.
19 S. N. Jadhav and C. V. Rode, An efficient palladium catalyzed Mizoroki–Heck cross-coupling in water, *Green Chem.*, 2017, **19**(24), 5958–5970.
20 J. Sherwood, J. H. Clark, I. J. S. Fairlamb and J. M. Slattery, Solvent effects in palladium catalysed cross-coupling reactions, *Green Chem.*, 2019, **21**(9), 2164–2213.
21 D. n. Fodor, T. s. Kégl, J. z. M. Tukacs, A. K. Horváth and L. s. T. Mika, Homogeneous Pd-catalyzed Heck coupling in γ-valerolactone as a green reaction medium: a catalytic, kinetic, and computational study, *ACS Sustainable Chem. Eng.*, 2020, **8**(26), 9926–9936.
22 C. C. Cassol, A. P. Umpierre, G. Machado, S. I. Wolke and J. Dupont, The role of Pd nanoparticles in ionic liquid in the Heck reaction, *J. Am. Chem. Soc.*, 2005, **127**(10), 3298–3299.
23 M. Dohendou, K. Pakzad, Z. Nezafat, M. Nasrollahzadeh and M. G. Dekamin, Progresses in chitin, chitosan, starch, cellulose, pectin, alginate, gelatin and gum based (nano) catalysts for the Heck coupling reactions: A review, *Int. J. Biol. Macromol.*, 2021, **192**, 771–819.
24 F. Valentini, L. Carpisassi, A. Comès, C. Aprile and L. Vaccaro, Tailor-Made POLITAG-Pd0 Catalyst for the Low-Loading Mizoroki–Heck Reaction in γ-Valerolactone as a Safe Reaction Medium, *ACS Sustainable Chem. Eng.*, 2022, **10**(37), 12386–12393.
25 S. Ashiri and E. Mehdipour, Preparation of a novel palladium catalytic hydrogel based on graphene oxide/chitosan NPs and cellulose nanowhiskers, *RSC Adv.*, 2018, **8**(57), 32877–32885.
26 A. Wolfson, S. Biton and O. Levy-Ontman, Study of Pd-based catalysts within red algae-derived polysaccharide supports in a Suzuki cross-coupling reaction, *RSC Adv.*, 2018, **8**(66), 37939–37948.
27 C.-A. Wang, K. Nie, G.-D. Song, Y.-W. Li and Y.-F. Han, Phenanthroline-based microporous organic polymer as a platform for an immobilized palladium catalyst for organic transformations, *RSC Adv.*, 2019, **9**(15), 8239–8245.
28 W. Xu, C. Liu, D. Xiang, Q. Luo, Y. Shu, H. Lin, Y. Hu, Z. Zhang and Y. Ouyang, Palladium catalyst immobilized on functionalized microporous organic polymers for C–C coupling reactions, *RSC Adv.*, 2019, **9**(59), 34595–34600.
29 D. Rohleder and P. Vana, Mesoporous-silica-coated palladium-nanocubes as recyclable nanocatalyst in C–C-coupling reaction – a green approach, *RSC Adv.*, 2020, **10**(44), 26504–26507.
30 J. Cárdenas, R. Gaviño, E. García-Ríos, L. Rios-Ruiz, A. C. Puello-Cruz, F. N. Morales-Serna, S. Gómez, A. López-Torres and J. A. Morales-Serna, The Heck reaction of allylic alcohols catalysed by an N-heterocyclic carbene-Pd(ii) complex and toxicity of the ligand precursor for the marine benthic copepod Amphiascoides atopus, *RSC Adv.*, 2021, **11**(33), 20278–20284.
31 S. Sheikh, M. A. Nasseri, M. Chahkandi, O. Reiser and A. Allahresani, Dendritic structured palladium complexes: magnetically retrievable, highly efficient heterogeneous nanocatalyst for Suzuki and Heck cross-coupling reactions, *RSC Adv.*, 2022, **12**(15), 8833–8840.
32 I. Raya, S. Danshina, A. T. Jalil, W. Suksatan, M. Z. Mahmoud, A. B. Roomi, Y. F. Mustafa and M. Kazemnejadi, Catalytic filtration: efficient C-C cross-coupling using Pd(II)-salen complex-embedded cellulose filter paper as a portable catalyst, *RSC Adv.*, 2022, **12**(31), 20156–20173.

33 A. Kumar, G. Kumar Rao and A. K Singh, Organochalcogen ligands and their palladium(ii) complexes: Synthesis to catalytic activity for Heck coupling, *RSC Adv.*, 2012, **2**(33), 12552–12574.

34 N. Norouzi, M. K. Das, A. J. Richard, A. A. Ibrahim, H. M. El-Kaderi and M. S. El-Shall, Heterogeneous catalysis by ultra-small bimetallic nanoparticles surpassing homogeneous catalysis for carbon–carbon bond forming reactions, *Nanoscale*, 2020, **12**(37), 19191–19202.

35 J. Guerra and M. A. Herrero, Hybrid materials based on Pd nanoparticles on carbon nanostructures for environmentally benign C–C coupling chemistry, *Nanoscale*, 2010, **2**(8), 1390–1400.

36 H. Joshi, K. N. Sharma, A. K. Sharma and A. K. Singh, Palladium–phosphorus/sulfur nanoparticles (NPs) decorated on graphene oxide: synthesis using the same precursor for NPs and catalytic applications in Suzuki–Miyaura coupling, *Nanoscale*, 2014, **6**(9), 4588–4597.

37 Y. Yang, C. E. Castano, B. F. Gupton, A. C. Reber and S. N. Khanna, A fundamental analysis of enhanced cross-coupling catalytic activity for palladium clusters on graphene supports, *Nanoscale*, 2016, **8**(47), 19564–19572.

38 K. Hong, M. Sajjadi, J. M. Suh, K. Zhang, M. Nasrollahzadeh, H. W. Jang, R. S. Varma and M. Shokouhimehr, Palladium nanoparticles on assorted nanostructured supports: applications for Suzuki, Heck, and Sonogashira cross-coupling reactions, *ACS Appl. Nano Mater.*, 2020, **3**(3), 2070–2103.

39 M. Nasrollahzadeh, S. M. Sajadi, A. Rostami-Vartooni and A. Azarian, Palladium nanoparticles supported on copper oxide as an efficient and recyclable catalyst for carbon (sp2)–carbon (sp2) cross-coupling reaction, *Mater. Res. Bull.*, 2015, **68**, 150–154.

40 F. Christoffel and T. R. Ward, Palladium-Catalyzed Heck Cross-Coupling Reactions in Water: A Comprehensive Review, *Catal. Lett.*, 2018, **148**(2), 489–511.

41 G. S. Lee, D. Kim and S. H. Hong, Pd-catalyzed formal Mizoroki–Heck coupling of unactivated alkyl chlorides, *Nat. Commun.*, 2021, **12**(1), 1–12.

42 A. Zebardasti, M. G. Dekamin and E. Doustkhah, The Isocyanurate-Carbamate-Bridged Hybrid Mesoporous Organosilica: An Exceptional Anchor for Pd Nanoparticles and a Unique Catalyst for Nitroaromatics Reduction, *Catalysts*, 2021, **11**(5), 621.

43 M. A. Gotthardt, A. Beilmann, R. Schoch, J. Engelke and W. Kleist, Post-synthetic immobilization of palladium complexes on metal–organic frameworks – a new concept for the design of heterogeneous catalysts for Heck reactions, *RSC Adv.*, 2013, **3**(27), 10676–10679.

44 A. Ghorbani-Choghamarani, B. Tahmasbi and P. Moradi, Synthesis of a new Pd (0)-complex supported on boehmite nanoparticles and study of its catalytic activity for Suzuki and Heck reactions in H 2 O or PEG, *RSC Adv.*, 2016, **6**(49), 43205–43216.

45 A. R. Hajipour, Z. Khorsandi and H. Farrokhpour, Regioselective Heck reaction catalyzed by Pd nanoparticles immobilized on DNA-modified MWCNTs, *RSC Adv.*, 2016, **6**(64), 59124–59130.

46 M. A. Zolfigol, T. Azadbakht, V. Khakyzadeh, R. Nejatyami and D. M. Perrin, C (sp 2)–C (sp 2) cross coupling reactions catalyzed by an active and highly stable magnetically separable Pd-nanocatalyst in aqueous media, *RSC Adv.*, 2014, **4**(75), 40036–40042.

47 G. Arora, M. Yadav, R. Gaur, R. Gupta, P. Yadav, R. Dixit and R. K. Sharma, Fabrication, functionalization and advanced applications of magnetic hollow materials in confined catalysis and environmental remediation, *Nanoscale*, 2021, **13**(25), 10967–11003.

48 S. R. Attar and S. B. Kamble, Recent advances in nanoparticles towards sustainability and their application in organic transformations in aqueous media, *Nanoscale*, 2022, **14**(45), 16761–16786.

49 M. Zvaigzne, P. Samokhvalov, Y. K. Gun'ko and I. Nabiev, Anisotropic nanomaterials for asymmetric synthesis, *Nanoscale*, 2021, **13**(48), 20354–20373.

50 H. J. Qiu, H.-T. Xu, L. Liu and Y. Wang, Correlation of the structure and applications of dealloyed nanoporous metals in catalysis and energy conversion/storage, *Nanoscale*, 2015, **7**(2), 386–400.

51 K. Hasan, C. Fowler, P. Kwong, A. K. Crane, J. L. Collins and C. M. Kozak, Synthesis and structure of iron (III) diamine-bis (phenolate) complexes, *Dalton Trans.*, 2008, (22), 2991–2998.

52 T. Baran and M. Nasrollahzadeh, Facile synthesis of palladium nanoparticles immobilized on magnetic biodegradable microcapsules used as effective and recyclable catalyst in Suzuki-Miyaura reaction and p-nitrophenol reduction, *Carbohydr. Polym.*, 2019, **222**, 115029.

53 N. Sharma, H. Ojha, A. Bharadwaj, D. P. Pathak and R. K. Sharma, Preparation and catalytic applications of nanomaterials: a review, *RSC Adv.*, 2015, **5**(66), 53381–53403.

54 K. Zhao, L.-X. Zhang, H. Xu, Y.-F. Liu, B. Tang and L.-J. Bie, Single-ion chelation strategy for synthesis of monodisperse Pd nanoparticles anchored in MOF-808 for highly efficient hydrogenation and cascade reactions, *Nanoscale*, 2022, **14**(30), 10980–10991.

55 T. Baran, I. Sargin, M. Kaya and A. Menteş, Green heterogeneous Pd (II) catalyst produced from chitosan-cellulose micro beads for green synthesis of biaryls, *Carbohydr. Polym.*, 2016, **152**, 181–188.

56 M. Chtchigrovsky, A. Primo, P. Gonzalez, K. Molvinger, M. Robitzer, F. Quignard and F. Taran, Functionalized chitosan as a green, recyclable, biopolymer-supported catalyst for the [3+ 2] Huisgen cycloaddition, *Angew. Chem., Int. Ed.*, 2009, **48**(32), 5916–5920.

57 Z. Zhou, C. Lu, X. Wu and X. Zhang, Cellulose nanocrystals as a novel support for CuO nanoparticles catalysts: facile synthesis and their application to 4-nitrophenol reduction, *RSC Adv.*, 2013, **3**(48), 26066–26073.

58 A. Pourjavadi, A. Motamedi, S. H. Hosseini and M. Nazari, Magnetic starch nanocomposite as a green heterogeneous

support for immobilization of large amounts of copper ions: heterogeneous catalyst for click synthesis of 1, 2, 3-triazoles, *RSC Adv.*, 2016, **6**(23), 19128–19135.

59 Z. Kheilkordi, G. M. Ziarani, A. Badiei and M. Sillanpää, Recent advances in the application of magnetic bio-polymers as catalysts in multicomponent reactions, *RSC Adv.*, 2022, **12**(20), 12672–12701.

60 A. R. Hajipour, F. Rezaei and Z. Khorsandi, Pd/Cu-free Heck and Sonogashira cross-coupling reaction by Co nanoparticles immobilized on magnetic chitosan as reusable catalyst, *Green Chem.*, 2017, **19**(5), 1353–1361.

61 S. S. Ray and M. Bousmina, Biodegradable polymers and their layered silicate nanocomposites: in greening the 21st century materials world, *Prog. Mater. Sci.*, 2005, **50**(8), 962–1079.

62 J. K. Pandey, A. P. Kumar, M. Misra, A. K. Mohanty, L. T. Drzal and R. Palsingh, Recent advances in biodegradable nanocomposites, *J. Nanosci. Nanotechnol.*, 2005, **5**(4), 497–526.

63 M. Madrahalli Bharamanagowda and R. K. Panchangam, Fe3O4-Lignin@ Pd-NPs: A highly efficient, magnetically recoverable and recyclable catalyst for Mizoroki-Heck reaction under solvent-free conditions, *Appl. Organomet. Chem.*, 2020, **34**(10), e5837.

64 R. Hassandoost, S. R. Pouran, A. Khataee, Y. Orooji and S. W. Joo, Hierarchically structured ternary heterojunctions based on Ce3+/Ce4+ modified Fe3O4 nanoparticles anchored onto graphene oxide sheets as magnetic visible-light-active photocatalysts for decontamination of oxytetracycline, *J. Hazard. Mater.*, 2019, **376**, 200–211.

65 Y. Orooji, M. Ghanbari, O. Amiri and M. Salavati-Niasari, Facile fabrication of silver iodide/graphitic carbon nitride nanocomposites by notable photo-catalytic performance through sunlight and antimicrobial activity, *J. Hazard. Mater.*, 2020, **389**, 122079.

66 Z. Taherian, A. Khataee and Y. Orooji, Facile synthesis of yttria-promoted nickel catalysts supported on MgO-MCM-41 for syngas production from greenhouse gases, *Renewable Sustainable Energy Rev.*, 2020, **134**, 110130.

67 O. Levy-Ontman, S. Biton, B. Shlomov and A. Wolfson, Renewable polysaccharides as supports for palladium phosphine catalysts, *Polymers*, 2018, **10**(6), 659.

68 M. G. Dekamin, M. Azimoshan and L. Ramezani, Chitosan: a highly efficient renewable and recoverable bio-polymer catalyst for the expeditious synthesis of α-amino nitriles and imines under mild conditions, *Green Chem.*, 2013, **15**(3), 811–820.

69 A. El Kadib, Chitosan as a sustainable organocatalyst: a concise overview, *ChemSusChem*, 2015, **8**(2), 217–244.

70 M. G. Dekamin, E. Kazemi, Z. Karimi, M. Mohammadalipoor and M. R. Naimi-Jamal, Chitosan: An efficient biomacromolecule support for synergic catalyzing of Hantzsch esters by CuSO4, *Int. J. Biol. Macromol.*, 2016, **93**, 767–774.

71 S. Zhong, Preparation of chitosan/poly (methacrylic acid) supported palladium nanofibers as an efficient and stable catalyst for Heck reaction, *J. Chem. Sci.*, 2020, **132**(1), 1–9.

72 K. Hasan, Methyl salicylate functionalized magnetic chitosan immobilized palladium nanoparticles: an efficient catalyst for the Suzuki and Heck coupling reactions in water, *ChemistrySelect*, 2020, **5**(23), 7129–7140.

73 S. Sadjadi, M. M. Heravi and M. Raja, Composite of ionic liquid decorated cyclodextrin nanosponge, graphene oxide and chitosan: a novel catalyst support, *Int. J. Biol. Macromol.*, 2019, **122**, 228–237.

74 Y. Du, S. Wei, M. Tang, M. Ye, H. Tao, C. Qi and L. Shao, Palladium nanoparticles stabilized by chitosan/PAAS nanofibers: A highly stable catalyst for Heck reaction, *Appl. Organomet. Chem.*, 2020, **34**(5), e5619.

75 E. Valiey, M. G. Dekamin and Z. Alirezvani, Melamine-modified chitosan materials: An efficient and recyclable bifunctional organocatalyst for green synthesis of densely functionalized bioactive dihydropyrano[2,3-c]pyrazole and benzylpyrazolyl coumarin derivatives, *Int. J. Biol. Macromol.*, 2019, **129**, 407–421.

76 Z. Alirezvani, M. G. Dekamin and E. Valiey, Cu (II) and magnetite nanoparticles decorated melamine-functionalized chitosan: A synergistic multifunctional catalyst for sustainable cascade oxidation of benzyl alcohols/Knoevenagel condensation, *Sci. Rep.*, 2019, **9**(1), 17758.

77 B. E. Teixeira-Costa and C. T. Andrade, Chitosan as a valuable biomolecule from seafood industry waste in the design of green food packaging, *Biomolecules*, 2021, **11**(11), 1599.

78 D. Naghipour, J. Jaafari, S. D. Ashrafi and A. H. Mahvi, Remediation of heavy metals contaminated silty clay loam soil by column extraction with ethylenediaminetetraacetic acid and nitrilo triacetic acid, *J. Environ. Eng.*, 2017, **143**(8), 04017026.

79 T. Yu, Z. Xue, X. Zhao, W. Chen and T. Mu, Green synthesis of porous β-cyclodextrin polymers for rapid and efficient removal of organic pollutants and heavy metal ions from water, *New J. Chem.*, 2018, **42**(19), 16154–16161.

80 K. Zhang, Z. Dai, W. Zhang, Q. Gao, Y. Dai, F. Xia and X. Zhang, EDTA-based adsorbents for the removal of metal ions in wastewater, *Coord. Chem. Rev.*, 2021, **434**, 213809.

81 F. Zhao, E. Repo, D. Yin, L. Chen, S. Kalliola, J. Tang, E. Iakovleva, K. C. Tam and M. Sillanpää, One-pot synthesis of trifunctional chitosan-EDTA-β-cyclodextrin polymer for simultaneous removal of metals and organic micropollutants, *Sci. Rep.*, 2017, **7**(1), 1–14.

82 K. Khomthawee, N. Nilada, A. Homchuen and P. Saejueng, Chitosan-EDTA-palladium composite for the Suzuki-Miyaura reaction, *Appl. Organomet. Chem.*, 2022, e6987.

83 E. Valiey, M. G. Dekamin and S. Bondarian, Sulfamic acid grafted to cross-linked chitosan by dendritic units: a bio-based, highly efficient and heterogeneous organocatalyst for green synthesis of 2, 3-dihydroquinazoline derivatives, *RSC Adv.*, 2023, **13**(1), 320–334.

84 N. Rostami, M. Dekamin, E. Valiey and H. Fanimoghadam, Chitosan-EDTA-Cellulose network as a green, recyclable and multifunctional biopolymeric organocatalyst for the one-pot synthesis of 2-amino-4H-pyran derivatives, *Sci. Rep.*, 2022, **12**(1), 8642.
85 N. Rostami, M. G. Dekamin and E. Valiey, Chitosan-EDTA-Cellulose bio-based network: A recyclable multifunctional organocatalyst for green and expeditious synthesis of Hantzsch esters, *Carbohydr. Polym. Technol. Appl.*, 2023, **5**, 100279.
86 P. G. de Abrantes, I. F. Costa, N. K. d. S. M. Falcão, J. M. G. de Oliveira Ferreira, C. G. L. Junior, E. E. d. S. Teotonio and J. A. Vale, The Efficient Knoevenagel Condensation Promoted by Bifunctional Heterogenized Catalyst Based Chitosan-EDTA at Room Temperature, *Catal. Lett.*, 2022, 1–11.
87 E. Valiey and M. G. Dekamin, Supported copper on a diamide–diacid-bridged PMO: an efficient hybrid catalyst for the cascade oxidation of benzyl alcohols/Knoevenagel condensation, *RSC Adv.*, 2022, **12**(1), 437–450.
88 L.-N. Vauquelin and P. J. Robiquet, The discovery of a new plant principle in Asparagus sativus, *Ann. Chim.*, 1806, **57**(88–93), 14.
89 M. Delaville, Sur les seves d'asperges et de choux, *Ann. Chim.*, 1802, 298.
90 P. J. Lea, L. Sodek, M. A. Parry, P. R. Shewry and N. G. Halford, Asparagine in plants, *Ann. Appl. Biol.*, 2007, **150**(1), 1–26.
91 X. Wang, T. Gao, M. Yang, J. Zhao, F.-L. Jiang and Y. Liu, Microwave-assisted synthesis, characterization, cell imaging of fluorescent carbon dots using l-asparagine as precursor, *New J. Chem.*, 2019, **43**(8), 3323–3331.
92 G. Saikia, K. Ahmed, C. Rajkhowa, M. Sharma, H. Talukdar and N. S. Islam, Polymer immobilized tantalum (v)–amino acid complexes as selective and recyclable heterogeneous catalysts for oxidation of olefins and sulfides with aqueous H 2 O 2, *New J. Chem.*, 2019, **43**(44), 17251–17266.
93 M. Sova, Antioxidant and antimicrobial activities of cinnamic acid derivatives, *Mini-Rev. Med. Chem.*, 2012, **12**(8), 749–767.
94 E. Pontiki, D. Hadjipavlou-Litina, K. Litinas and G. Geromichalos, Novel cinnamic acid derivatives as antioxidant and anticancer agents: Design, synthesis and modeling studies, *Molecules*, 2014, **19**(7), 9655–9674.
95 N. Ruwizhi and B. A. Aderibigbe, Cinnamic acid derivatives and their biological efficacy, *Int. J. Mol. Sci.*, 2020, **21**(16), 5712.
96 A. Gunia-Krzyżak, K. Słoczyńska, J. Popiół, P. Koczurkiewicz, H. Marona and E. Pękala, Cinnamic acid derivatives in cosmetics: current use and future prospects, *Int. J. Cosmet. Sci.*, 2018, **40**(4), 356–366.
97 P. Sharma, Cinnamic acid derivatives: a new chapter of various pharmacological activities, *J. Chem. Pharm. Res.*, 2011, **3**(2), 403–423.
98 A. Peperidou, E. Pontiki, D. Hadjipavlou-Litina, E. Voulgari and K. Avgoustakis, Multifunctional cinnamic acid derivatives, *Molecules*, 2017, **22**(8), 1247.
99 S. Bhatia, G. Wellington, J. Cocchiara, J. Lalko, C. Letizia and A. Api, Fragrance material review on butyl cinnamate, *Food Chem. Toxicol.*, 2007, **45**(1), S49–S52.
100 M. Batory and H. Rotsztejn, Shikimic acid in the light of current knowledge, *J. Cosmet. Dermatol.*, 2022, **21**(2), 501–505.
101 E. M. da Silva, H. D. Vidal and A. G. Corrêa, Advances on Greener asymmetric synthesis of antiviral drugs via organocatalysis, *Pharmaceuticals*, 2021, **14**(11), 1125.
102 W. H. Perkin, XI.—On the formation of coumarin and of cinnamic and of other analogous acids from the aromatic aldehydes, *J. Chem. Soc.*, 1877, **31**, 388–427.
103 G.-S. Lee, A. Widjaja and Y.-H. Ju, Enzymatic synthesis of cinnamic acid derivatives, *Biotechnol. Lett.*, 2006, **28**(8), 581–585.
104 A. Mobinikhaledi, N. Foroughifar and H. F. Jirandehi, Microwave–assisted synthesis of cinnamic acid derivatives in the presence of PPE and under solvent-free condition, *Synth. React. Inorg., Met.-Org., Nano-Met. Chem.*, 2008, **38**(5), 428–430.
105 M. Gupta and B. P. Wakhloo, Tetrabutylammoniumbromide mediated Knoevenagel condensation in water: Synthesis of cinnamic acids, *Arkivoc*, 2007, **2007**, 94–98.
106 A. Avanesyan, A. Simonyan and M. Simonyan, Phosphorus Oxychloride in Organic Synthesis. Part 3: Synthesis of α-Benzoylaminocinnamic Acids, *Pharm. Chem. J.*, 2005, **39**(7), 379–380.
107 B. P. Joshi, A. Sharma and A. K. Sinha, Efficient one-pot, two-step synthesis of (E)-cinnmaldehydes by dehydrogenation–oxidation of arylpropanes using DDQ under ultrasonic irradiation, *Tetrahedron*, 2006, **62**(11), 2590–2593.
108 G. V. Ambulgekar, B. M. Bhanage and S. D. Samant, Low temperature recyclable catalyst for Heck reactions using ultrasound, *Tetrahedron Lett.*, 2005, **46**(14), 2483–2485.
109 E. Valiey and M. G. Dekamin, Pyromellitic diamide–diacid bridged mesoporous organosilica nanospheres with controllable morphologies: a novel PMO for the facile and expeditious synthesis of imidazole derivatives, *Nanoscale Adv.*, 2022, **4**(1), 294–308.
110 S. Safapoor, M. G. Dekamin, A. Akbari and M. R. Naimi-Jamal, Synthesis of (E)-2-(1H-tetrazole-5-yl)-3-phenylacrylenenitrile derivatives catalyzed by new ZnO nanoparticles embedded in a thermally stable magnetic periodic mesoporous organosilica under green conditions, *Sci. Rep.*, 2022, **12**(1), 10723.
111 S. Fujita and N. Sakairi, Water soluble EDTA-linked chitosan as a zwitterionic flocculant for pH sensitive removal of Cu (II) ion, *RSC Adv.*, 2016, **6**(13), 10385–10392.
112 N. Arsalani and S. Z. Mousavi, Synthesis and characterization of water-soluble and carboxy-functional polyester and polyamide based on ethylenediaminetetraacetic acid and their metal complexes, *Iran. Polym. J.*, 2003, **12**(4), 291–296.
113 S. Kumar and J. Koh, Physiochemical, optical and biological activity of chitosan-chromone derivative for

biomedical applications, *Int. J. Mol. Sci.*, 2012, **13**(5), 6102–6116.

114 J. Sherwood, J. H. Clark, I. J. Fairlamb and J. M. Slattery, Solvent effects in palladium catalysed cross-coupling reactions, *Green Chem.*, 2019, **21**(9), 2164–2213.

115 A. Jutand, Dual role of nucleophiles in palladium-catalyzed Heck, Stille, and Sonogashira reactions, *Pure Appl. Chem.*, 2004, **76**(3), 565–576.

116 J. A. Molina de la Torre, P. Espinet and A. C. Albeniz, Solvent-induced reduction of palladium-aryls, a potential interference in Pd catalysis, *Organometallics*, 2013, **32**(19), 5428–5434.

117 A. Carral-Menoyo, N. Sotomayor and E. Lete, Palladium-catalysed Heck-type alkenylation reactions in the synthesis of quinolines. Mechanistic insights and recent applications, *Catal. Sci. Technol.*, 2020, **10**(16), 5345–5361.

118 F. Jafarpour, N. Jalalimanesh, M. Teimouri and M. Shamsianpour, Palladium/norbornene chemistry: an unexpected route to methanocarbazole derivatives via three Csp 3–Csp 2/Csp 3–N/Csp 2–N bond formations in a single synthetic sequence, *Chem. Commun.*, 2015, **51**(1), 225–228.

119 A. M. Alazemi, K. M. Dawood, H. M. Al-Matar and W. M. Tohamy, Efficient and Recyclable Solid-Supported Pd (II) Catalyst for Microwave-Assisted Suzuki Cross-Coupling in Aqueous Medium, *ACS Omega*, 2022, **7**(33), 28831–28848.

120 **https://www.guidechem.com/encyclopedia/trans-cinnamic-acid-dic3044.html**, trans-cinnamic acid.

121 **https://www.hzchempro.com/product/116868-96-3.html**, (E)-3-(4-acetylphenyl)acrylic acid.

122 **https://www.guidechem.com/dictionary/en/1896-62-4.html**, trans-4-Phenyl-3-buten-2-one.

123 **https://www.guidechem.com/encyclopedia/ethyl-cinnamate-dic1774.html**, ethyl cinnamate.

124 M. L. Kantam, P. Srinivas, J. Yadav, P. R. Likhar and S. Bhargava, Trifunctional N, N, O-terdentate amido/pyridyl carboxylate ligated Pd (II) complexes for Heck and Suzuki reactions, *J. Org. Chem.*, 2009, **74**(13), 4882–4885.

125 M. A. Fredricks, M. Drees and K. Köhler, Acceleration of the Rate of the Heck Reaction through UV- and Visible-Light-Induced Palladium(II) Reduction, *ChemCatChem*, 2010, **2**(11), 1467–1476.

126 C. Wu, X. Peng, L. Zhong, X. Li and R. Sun, Green synthesis of palladium nanoparticles via branched polymers: a bio-based nanocomposite for C–C coupling reactions, *RSC Adv.*, 2016, **6**(38), 32202–32211.

127 B. Karimi and D. Enders, New N-heterocyclic carbene palladium complex/ionic liquid matrix immobilized on silica: Application as recoverable catalyst for the Heck reaction, *Org. Lett.*, 2006, **8**(6), 1237–1240.

128 X. Cui, J. Li, Z.-P. Zhang, Y. Fu, L. Liu and Q.-X. Guo, Pd (quinoline-8-carboxylate) 2 as a low-priced, phosphine-free catalyst for Heck and Suzuki reactions, *J. Org. Chem.*, 2007, **72**(24), 9342–9345.

129 D. Lv and M. Zhang, O-carboxymethyl chitosan supported heterogeneous palladium and Ni catalysts for heck reaction, *Molecules*, 2017, **22**(1), 150.